Improving Tracking Performance of Industrial SCARA Robots Using a New Sliding Mode Control Algorithm

Min-Cheol Lee*, Kwon Son* and Jang-Myoung Lee**

(*Received July 18, 1997*)

This paper addresses the implementation of a new sliding mode control algorithm for high speed and high precision tasks, which is robust against variations in the robot parameters and load. The effects of nonlinear dynamics, which are difficult to model accurately, become prominent in high speed operations. This paper attempts to treat the nonlinear dynamics of a SCARA robot as a disturbance. Based upon this approach, a new sliding mode control algorithm is proposed, in which a switching control input can be obtained easily and is determined to satisfy the existence condition for sliding mode control. A graphic simulator is used to evaluate the proposed algorithm for a SCARA robot. Simulation results show that the proposed algorithm is robust against disturbances and can reduce the magnitude of chattering, which is an unavoidable problem in sliding mode control. Experiments are carried out to validate the simulated results with an industrial SCARA robot using DSPs.

Key Words: Sliding Mode Control, SCARA Robot, Digital Signal Processor, Signal Compression Method, Trajectory Control

1. Introduction

A PID algorithm has been used for control of most industrial robots. This algorithm, however, cannot provide high precision for high speed tasks where abrupt changes in dynamic parameters occur.

Unless the nonlinearities of robotic manipulators are properly compensated for, control performance is not satisfactory with a PID algorithm. Also, an accurate model of a robotic system is very difficult due to the nonlinear friction and changes in the load during task execution. As fast processors such as DSPs (digital signal processors) are developed, the nonlinear terms of robotic manipulators can be calculated in real-time (Nishimoto, 1985). Some research has been carried out using a PID control algorithm with nonlinear compensation based on a simplified dynamic model, but they still cannot allow a robot to follow a desired path accurately at high speeds (Fu *et. al*, 1987; Nishimoto, 1985).

To overcome the problems of the unmodeled dynamics involved in high speed tasks, many researchers have used sliding mode control, which is known to be robust against parameter variations and load changes (Dong and Shifan, 1996; Fruta and Tomiyama, 1996; Harashima *et al.*, 1986; Hashimoto *et al.*, 1987; Parra-Vega *et al.*, 1994; Young, 1978; Slotine, 1985; Utkin, 1978; Wang *et al.*, 1994). Lee and Aoshima (1993) proposed an algorithm where the unmodeled dynamic terms were considered as an external disturbance, and applied their sliding mode control algorithm to three d. o. f. robots. Their algorithm suffered from inherent chattering caused by excessive switching inputs around the sliding surface.

This study proposes a new sliding mode control algorithm which reduces chattering in the presence of nonlinear terms and is robust against

* Division of Mechanical Engineering and Research Institute of Mechanical Technology, Pusan National University

** Department of Electronics Engineering and Research Institute of Mechanical Technology, Pusan National University

variations in the parameters and payload. The implementation of this algorithm in a SCARA robot is easier than other dynamic algorithms, since all the nonlinear terms are treated as a disturbance. A three-dimensional graphic simulator was used for the comparison of different algorithms (K. Son, *et al.* 1994). The performance of the suggested algorithm is compared to that of the computed torque algorithm in the simulator. The validity of the control algorithm is demonstrated in a real environment where parameter variations exist. Experimental results demonstrate that the proposed algorithm is accurate and robust. The success in controlling the SCARA robot implies that the algorithm is applicable to the real-time control of industrial robots using DSPs.

2. Controller Design

2.1 Dynamic model

A four-axes SCARA robot is shown in Fig. 1. The forward kinematics are obtained using the Denavit-Hartenberg representation and the equations of motion are derived from the Lagrange-Euler equations as follows:

$$H_{11}\ddot{\theta}_1+H_{12}\ddot{\theta}_2+H_{14}\ddot{\theta}_4+h_{112}\dot{\theta}_1\dot{\theta}_2+h_{122}\dot{\theta}_2^2+\nu_1\dot{\theta}_1+k_1sgn(\dot{\theta}_1)=\tau_1 \quad (1)$$

$$H_{21}\ddot{\theta}_1+H_{22}\ddot{\theta}_2+H_{24}\ddot{\theta}_4+H_{211}\dot{\theta}_1^2+H_{212}\dot{\theta}_1\dot{\theta}_2+h_{221}\dot{\theta}_1\dot{\theta}_2+\nu_2\dot{\theta}_2+k_2sgn(\dot{\theta}_2)=\tau_2 \quad (2)$$

$$H_{33}\ddot{d}_3+G_3+\nu_3\dot{d}_3+k_3sgn(\dot{d}_3)=\tau_3 \quad (3)$$

$$H_{41}\ddot{\theta}_1+H_{42}\ddot{\theta}_2+H_{44}\ddot{\theta}_4+\nu_4\dot{\theta}_4+k_4sgn(\dot{\theta}_4)=\tau_4 \quad (4)$$

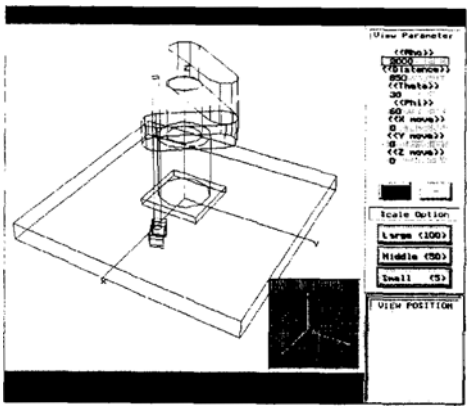

Fig. 1 SCARA robot.

where $H_{ij}\ddot{\theta}_j$, $h_{ijk}\dot{\theta}_j\dot{\theta}_k$, G_3, $\nu_i\dot{\theta}_i$, and $k_isgn(\dot{\theta}_i)$ are the inertial force, Coriolis and centrifugal forces, gravity force, viscous friction, and Coulomb friction terms, respectively. The detailed expressions of all terms are listed in the appendix.

The dynamic equations of an actuator for each joint can be written as

$$J_{mi}\ddot{\theta}_{mi}+B_{mi}\dot{\theta}_{mi}+\tau_{mi}=u_i \quad (5)$$

where J_{mi}, B_{mi}, τ_{mi}, and u_i are the moment of inertia, viscous damping coefficient, equivalent driving torque, and control input voltage, respectively. The nonlinear dynamic terms in Eqs. (1) to (5) are replaced by the disturbance F_i, and the simplified dynamic equations of the whole system can be written as

$$J_i\ddot{\theta}_i+B_i\dot{\theta}+F_i=k_iu_i \quad (6)$$

where θ_i is the rotaion angle of the ith link ; J_i is the linear equivalent inertia of the ith link including the ith motor shaft and reduction gears; B_i is the equivalent damping coefficient of the ith motor and reduction gears ; and k_i is a constant to be determined that reflects the motor torque coefficient, gear, reduction rate and armature resistance.

2.2 Sliding mode control

The sliding mode control ler is based on variable structure systems (VSS) and is characterized by a discontinuous control which changes "structure" upon reaching a set of predetermined switching surfaces in the state space (Utkin, 1978). The sliding mode controller is robust against parameter uncertainties, nonlinear components, change of parameters, etc. When switching delays are present, however, the trajectories chatter around the switching surfaces (Young, 1978). In this section, a new sliding mode control algorithm is proposed for robust control with less chattering, even though nonlinear terms are included as a disturbance.

To design a sliding mode control for a multi-input system, the general equation in state space is considered as follows:

$$\dot{\chi}=f(\chi,\ t)+B(\chi,\ t)\ u \quad (7)$$
$$\chi\in R^n \text{ and } u\in R^n$$

where χ is a state vector and u is a control input vector. When the ith switching surface is $s_i(\chi)=0$, the ith component u_i of u is selected as

$$u_i=\begin{cases} u_i^+(\chi,\ t) & \text{if } s_i(\chi)>0 \\ u_i^-(\chi,\ t) & \text{if } s_i(\chi)<0 \end{cases} \quad (i=1,\ \cdots,\ m). \tag{8}$$

The sliding mode in a multi-input system does not occur in $s_i(\chi)=0$, but in $\boldsymbol{s}(\boldsymbol{\chi})=(s_1,\ s_2,\ \cdots,\ s_m)=0$. For sliding mode control with multiple inputs, the control hierarchy method is selected because of its robustness properties similar to the design of a single input VSS. In the control hierarchy method, each switching plane satisfies one by one the existence condition of a sliding mode, $s_i(\chi)=0$, from a higher order hierarchy to a lower one (Utkin, 1978 ; Young, 1978 ; Harashima, *et al.*, 1986). By a hierarchy of switching planes, the sliding mode occurs on higher switching planes in the hierarchy. However, the condition $s_i(\chi)=0$ is not feasible for real systems. In this paper, a quasi-sliding mode control is used where the sliding mode of higher order hierarchy occurs in $|s_i(\chi)|<\varepsilon$ instead of $s_i(\chi)=0$.

For a control system to be in sliding mode, the system should satisfy the existence condition (Utkin, 1978; Young, 1978; Slotine, 1985; Harashima, *et al.*, 1986). For systems with a disturbance as in Eq. (6), a control input M can satisfy the existence condition only if the maximum disturbance value F_i is known and the input M can suppress a disturbance (Utkin, 1978; Harashima, *et al.*, 1986). However, a consequent problem is that increased chattering is unavoidable due to the larger value of M (Lee, M. C. and Aoshima, N., 1993).

This paper proposes a new algorithm for easier application of the sliding mode controller by using Eq. (6) to reduce chattering and suppress disturbances.

Let the desired angle, angular velocity, and angular acceleration of the ith joint be denoted by θ_{di}, $\dot{\theta}_{di}$, and $\ddot{\theta}_{di}$, respectively, and the corresponding measured angular quantities denoted by θ_i, $\dot{\theta}_{di}$, and $\ddot{\theta}_{di}$, respectively. The errors can be defined as

$$e_i=\theta_i-\theta_{di},\ \dot{e}_i=\dot{\theta}_i-\dot{\theta}_{di},\ \text{and}\ \ddot{e}_i=\ddot{\theta}_i-\ddot{\theta}_{di} \tag{9}$$

A switching line for the sliding mode can be expressed as

$$s_i=c_ie_i+\dot{e}_i \tag{10}$$

where s_i is the ith switching line and c_i is the corresponding slope.

From Eqs. (6) and (8) the existence condition of the sliding mode can be derived as

$$\begin{aligned} s_i\dot{s}_i &= s_i(c_i\dot{e}_i+\ddot{e}_i) \\ &= s_i\Big[c_i(s_i-c_ie_i)+\frac{1}{J_i}\{(k_iu_i \\ &\quad -B_i(\dot{e}_i+\dot{\theta}_{di})-F_i\}-\ddot{\theta}_{di}\Big] \\ &= s_i^2\Big(c_i-\frac{B_i}{J_i}\Big)+s_i\Big\{c_i-\frac{B_i}{J_i}\Big)c_ie_i \\ &\quad +\frac{k_iu_i}{J_i}-\frac{B_i}{J_i}\dot{\theta}_{di}-\frac{F_i}{J_i}-\ddot{\theta}_{di}\Big)\Big\}<0 \end{aligned} \tag{11}$$

To satisfy inequality (11) when $c_i<B_i/J_i$, the following relations are necessary.

$$\begin{aligned} &\frac{k_iu_i^+}{J_i}<\Big(c_i-\frac{B_i}{J_i}\Big)c_ie_i+\frac{F_i}{J_i}+\frac{B_i}{J_i}\dot{\theta}_{di} \\ &+\ddot{\theta}_{di} \quad \text{if } s_i>0 \\ &\frac{k_iu_i^-}{J_i}>\Big(c_i-\frac{B_i}{J_i}\Big)c_ie_i+\frac{F_i}{J_i}+\frac{B_i}{J_i}\dot{\theta}_{di} \\ &+\ddot{\theta}_{di} \quad \text{if } s_i<0 \end{aligned} \tag{12}$$

If relations (12) are satisfied, the sliding mode occurs because $s_i\dot{s}_i$ always becomes negative. When $c_i<B_i/J_i$, the ith joint control input u_i which satisfies relations (12) is obtained as follows:

$$u_i=\phi_{\alpha i}e_i+\phi_{fi}+\phi_{\beta i}\dot{\theta}_{di}+\phi_{\gamma i}\ddot{\theta}_{di} \tag{13}$$

where

$$\phi_{\alpha i}=\begin{cases} \alpha_i & \text{if } s_ie_i>0 \\ -\alpha_i & \text{if } s_ie_i<0 \end{cases}$$

$$\phi_{fi}=\begin{cases} u_{fi}^- & \text{if } s_i>0 \\ u_{fi}^+ & \text{if } s_i<0 \end{cases}$$

$$\phi_{\beta i}=\begin{cases} \beta_i & \text{if } s_i\ \dot{\theta}_{di}>0 \\ -\beta_i & \text{if } s_i\ \dot{\theta}_{di}<0 \end{cases}$$

$$\phi_{\gamma i}=\begin{cases} \gamma_i & \text{if } s_i\ \ddot{\theta}_{di}>0 \\ -\gamma_i & \text{if } s_i\ \ddot{\theta}_{di}<0 \end{cases}$$

$$\phi_{fi}=\begin{cases} u_{fi}^-=M_{1i}+M_{2i}f(e_i) & \text{if } s_i>0 \\ u_{fi}^+=-M_{1i}-M_{2i}f(e_i) & \text{if } s_i<0 \end{cases}, \text{ and}$$

$$f(e_i)=|e_i|$$

where $\phi_{\beta i}$ and $\phi_{\gamma i}$ are introduced to represent the feed forward control input terms which ensure the existence condition of the sliding mode against unfavorable effects of $\dot{\theta}_{di}$ and $\ddot{\theta}_{di}$ on trajectory

tracking. ϕ_{fi} is the modified control input not only for suppressing disturbances but also for decreasing chattering. The magnitude of the nonlinear terms in Eq. (6) is assumed to decrease as the error converges to zero. Therefore the value of M_{2i} in ϕ_{fi} is proportional to the absolute value of the error influencing the chattering magnitude. That is, ϕ_{fi} can be smaller because the magnitude of nonlinear terms related to the tracking error is smaller as the trajectory converges to a desired trajectory. Therefore, the smaller supplied ϕ_{fi} reduces chattering. The value of M_{1i} in ϕ_{fi} is selected based on the maximum value of F_i.

Other possible causes of chattering are sudden changes in velocity around a switching line. To decrease these changes, M_{1i} is chosen as

$$M_{1i}=\begin{cases} M_{1Si} & \text{if } s_i e_i<0 \\ M_{1Li} & \text{if } s_i e_i>0 \end{cases} \tag{14}$$

where M_{1i} is selected as the larger value M_{1Li} when it is supplied in the convergence direction to a desired trajectory, and the smaller value M_{1Si} is used in the opposite case.

There exists a sliding mode at joint i when the existence condition of $s_i\dot{s}_i<0$ is satisfied. The existence condition can be derived as

$$\begin{aligned} s_i\dot{s}_i &= s_i(c_i\dot{e}_i+\ddot{e}_i) \\ &= s_i^2\left(c_i-\frac{B_i}{J_i}\right)+s_ie_i\left(\frac{B_i}{J_i}c_i+\frac{k_i}{J_i}\phi_{\alpha i}-c_i^2\right) \\ &\quad +\left(\frac{k_i}{J_i}\phi_{fi}-\frac{F_i}{J_i}\right)s_i+\left(\frac{k_i}{J_i}\phi_{\beta i}-\frac{B_i}{J_i}\right)s_i\dot{\theta}_{di} \\ &\quad +\left(\frac{k_i}{J_i}\phi_{\gamma i}-1\right)s_i\ddot{\theta}_{di}<0 \end{aligned} \tag{15}$$

If each term in inequality (15) is negative, the existence condition is always satisfied. Equation (15) can be used to obtain the maximum values of the switching parameters in Eq. (13).

For a multi-input sliding mode control, the switching control input given by Eq. (13) should be supplied by a hierarchical control method. The control hierarchy used in this study is the hybrid method which can eliminate both gravity effects and interactions between links. The method switches proportional control to sliding mode control for the links of lower order as the links of higher order enter quasi-sliding mode. That is, if the state variables of higher order satisfy $|s_i|<\varepsilon_i$, those of lower order enter sliding mode, and then all the state variables of the lowest order gradually enter sliding mode.

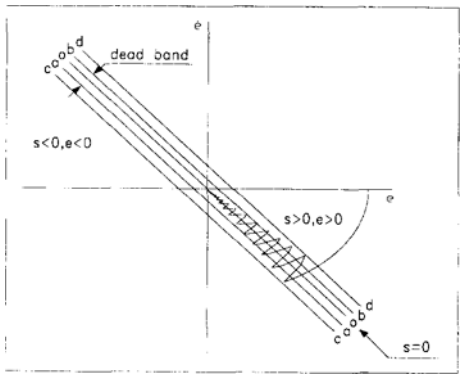

Fig. 2 Phase plane with a dead zone around the switching line.

However, in this case the chattering remains within a certain range because of the large M_{1i} although the state variables of the control system converge to a desired trajectory. In this study, to reduce this chattering, a high gain of M_{1i} is changed to a lower gain M_{1di} if a trajectory tracking error falls within a preset dead zone as shown in Fig. 2.

The phase plane for the error states of each link is shown in Fig. 2, where the line $o-o$ is a switching line of $s=0$. Lines $c-c$ and $d-d$ are the additional lines used to determine whether the higher order class converges to the sliding mode in hierarchical control. The magnitude of chattering is denoted by D, which is the distance between the switching line and the state variable and expressed as

$$D=\frac{|c_ie_i+\dot{e}_i|}{\sqrt{c_i^2+1}} \tag{16}$$

A dead zone is set and its width is described by $D=\varepsilon$ between lines $a-a$ and $b-b$ to reduce chattering. Reduction of chattering can be expected by changing the value of M_{1i} in ϕ_{fi} of the control input with a smaller one once the state variable falls into the dead zone.

2.3 Consideration of payload

Industrial robots for carrying objects experience changes of payload during assembly work.

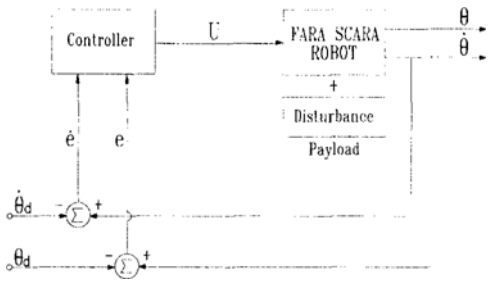

Fig. 3 Control block diagram.

We replace the dynamic effects of each joint by a gripper mass, $\bar{m}$, assuming the effect as a change of payload. The control loop with the payload is shown in Fig. 3, where a control input U is derived from the existence condition to satisfy the sliding mode around the switching line with state variables e_i and $\dot{e}_i$. The same control input U is supplied to a robot, and a trajectory tracking performance of the controller is investigated by comparing control results in two cases, with the payload and without the payload. To investigate the effect of an added payload, a payload $\bar{m}$ attached to the gripper. The dynamic terms affected by the added payload $\bar{m}$ are denoted by attaching the prefix 'A'. By adding payload $\bar{m}$, terms in Eqs. (1) to (4) are changed to

$$\begin{aligned}
AH_{11} &= \bar{m}(l_1^2 + l_2^2 + 2l_1l_2\cos\theta_2)\\
AH_{12} &= AH_{21} = \bar{m}(l_2^2 + 2l_1l_2\cos\theta_2)\\
AH_{22} &= \bar{m}l_2^2\\
AH_{33} &= \bar{m}\\
Ah_{112} &= -2\bar{m}l_1l_2\sin\theta_2\\
Ah_{122} &= -\bar{m}l_1l_2\sin\theta_2\\
Ah_{211} &= \bar{m}l_1l_2\sin\theta_2\\
Ah_{212} &= -\bar{h}_{221} = -0.5\bar{m}l_1l_2\sin\theta_2\\
AG_3 &= -\bar{m}g
\end{aligned} \tag{17}$$

3. Simulation

The proposed sliding mode control algorithm was evaluated on an off-line programming system. Specifications of the SCARA robot used in the simulation are listed in Table 1. The numerical integration was carried out using the fourth order Runge-Kutta method. Software was developed for simulation of the dynamic sliding mode control to cope with the time-varying disturbance F_i in Eq. (6). The developed software was transplanted to the off-line programming system. Quantitative and graphical comparisons between the proposed sliding mode control and the computed torque method were made.

Table 1 Specifications of SCARA robot.

	Axis 1	Axis 2	Axis 3	Axis 4
Mass of link (kg)	15.07	8.99	1.50	1.00
Length of link (m)	0.35	0.30	0.40	0.07
Visicosity coefficient of link (gf•cm/rpm)	0.79	0.33	0.70	0.30
Inertia of motor (g cm sec^2)	0.51	0.14	0.09	0.023
Damping coefficient of motor (kgf-cm)	0.2	0.1	0.08	0.08
Electromotive force constant (V/krpm)	22.5	21.0	21.0	18.5
Torque constant (kgf-cm/A)	2.19	2.04	2.04	1.8

The multi-input sliding mode control of the manipulator was achieved by the hierarchical control method where link 1 has the highest order and the sliding mode occurs successively in the order of links 2, 3, and 4. The states in an error state space of each link are denoted as s_1, s_2, s_3, and s_4. The lower order link 2 is controlled by the proportional control input until state s_1 converges into ε. As soon as state s_1 of link 1 converges into ε, the sliding mode control input is supplied to link 2. It is supplied by the same method until the sliding mode control reaches the lowest link. The slopes of switching surfaces and parameters in Eq. (11) are shown in Table 2.

An illustrative example is given for a case when the end effector moves from the start point (250mm, 100mm, 20mm, 40°) to the end point (250mm, −100mm, 200mm, −40°) as in Fig. 4. The robot trajectory was planned on the off-line programming system to calculate the corresponding joint angles. These angles were then used as reference inputs to the trajectory tracking control.

The simulation results obtained by the computed torque method in the case of a free payload are shown in Fig. 5, and the results of the sliding

mode in the same conditions are shown in Fig. 6. The results show that both the computed torque method and the sliding mode control enable the end-effector to follow the desired trajectory accurately. However, in applications to die polishing by a polishing robot, which needs a large polishing force and should endure various torque changes, the trajectory tracking control by the computed torque method may be degraded due to payload change.

To evaluate the tracking performance in the case of payload changes, another simulation for a payload of 8 kg was performed with the whole control gain unchanged. The tracking errors obtained by the two control algorithms are shown in Figs. 7 and 8. It should be noted that different scales are used in the graphical representations. In the case of the computed torque method, the

Table 2 Switching parameters.

	Axis 1	Axis 2	Axis 3	Axis 4
C_i	15	15	12	20
ϕ_{ai}	800	850	1550	1550
M_{1Li}	−100	−80	−850	−150
M_{1Si}	−80	−70	−180	−40
M_{2i}	−50	−50	−50	−50

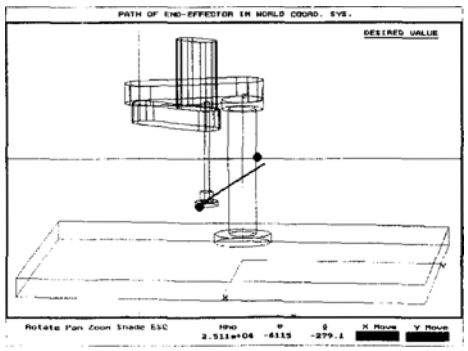

Fig. 4 Trajectory of end-effector.

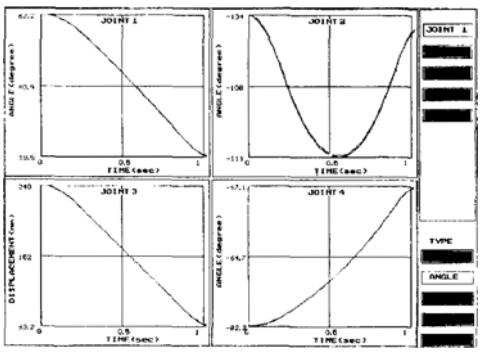

Fig. 5 Results of trajectory tracking by computed torque method.

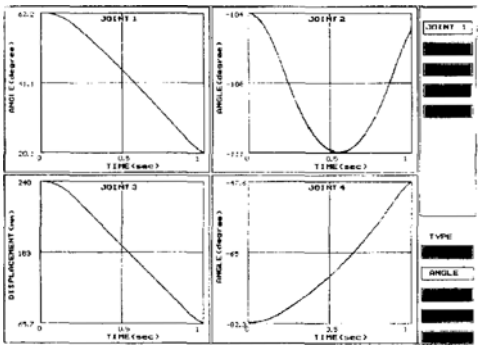

Fig. 6 Results of trajectory tracking by sliding mode control.

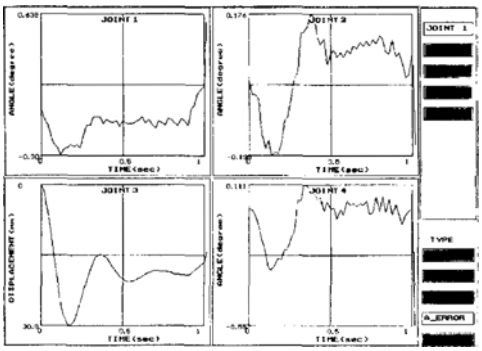

Fig. 7 Trajectory tracking errors by computed torque method in case of 8 kg payload.

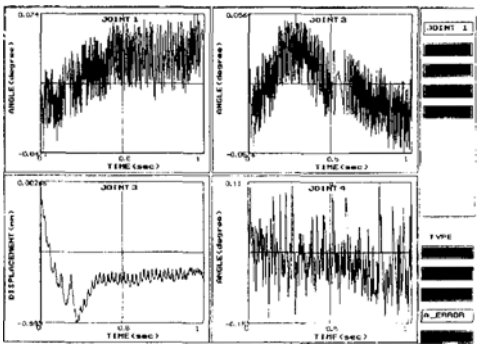

Fig. 8 Trajectory tracking errors by sliding mode control in case of 8 kg payload.

tracking errors increased except at joint 4. Particularly at joint 3, the maximum deviation from the desired trajectory reached 28 mm as can be seen in Fig. 7. However, in the case of sliding mode control, the maximum tracking error was only 0.75 mm at joint 3 as shown in Fig. 8. This demonstrates that the proposed control algorithm possesses robust tracking capabilities even when the nonlinear terms in Eqs. (1) to (5) are considered as a disturbance.

4. Experiment

Figure 9 shows a control system implemented in order to verify the performance of the proposed algorithm. A FARA robot (SM2) of SCARA type manufactured by Samsung Electronics Company was used in this study. A DSP board was used for the real-time signal processing to control the first two joints of the robot through the I/O board for two axes.

A PD control was selected as a reference control algorithm in order to compare the suggested sliding mode control. To obtain the best sets of parameters for the robot, the experiments on the step responses were carried out by trial and error. Figures 10, 11 show the best results among the step responses obtained for PD control of axes 1 and 2, respectively. The proper proportional and derivative gains of axes 1 and 2 were chosen as $K_{p1}=2$, $K_{d1}=0.25$, $K_{p2}=2$, $K_{d2}=0.375$, respectively. The chosen gains were used in trajectory tracking.

PD control was performed while the end-effector moved from the start point (400 mm, 150 mm) to the end point (400 mm, −130 mm) in the $x-y$ plane. Figure 12 shows the trajectory tracking result by PD control, which yielded a larger error maximum of about 5 mm.

To apply the sliding mode control to a real system, the boundary conditions of the switching surface need to be obtained. An ideal impulse is required to obtain the flat power spectrum in a wide frequency range. However, it is sufficient in practice for an impulse to have a flat power spectrum in a limited frequency range. The waveform of such an impulse can be Fourier -transformed and passed through a mathematical phase shift filter. The spectrum of the signal is

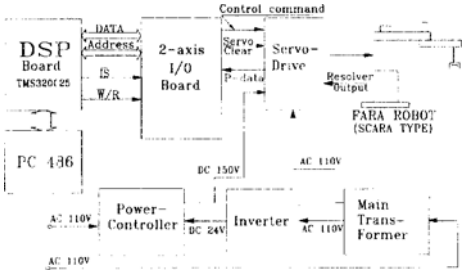

Fig. 9 Block diagram of control system.

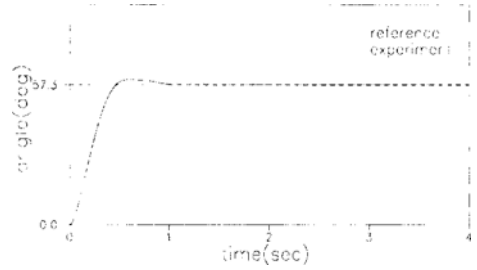

Fig. 10 Step response of axis 1 by PD control.

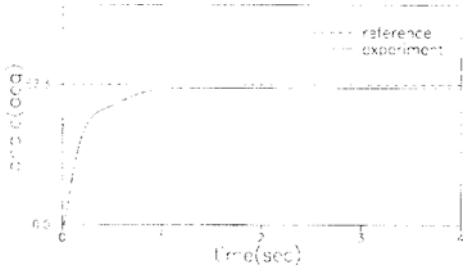

Fig. 11 Step response of axis 2 by PD control.

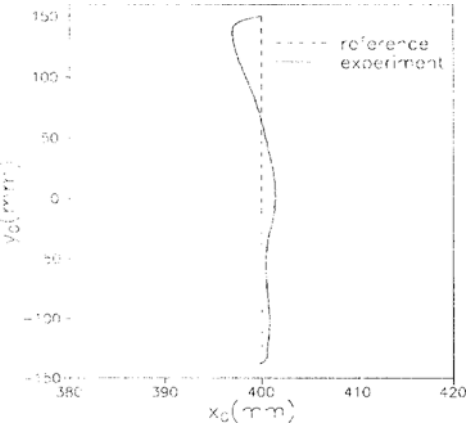

Fig. 12 Trajectory tracking by PD control.

constant in magnitude with the phase delay. If this signal is transformed into the time domain through the inverse Fourier transform, the test signal may have a lower amplitude and larger duration. The test signal is applied to the system whose parameters are to be estimated. A response obtained from the system with the input signal can be compressed through the FFT (fast Fourier transform), an inverse phase shift filter, and IFFT (inverse fast Fourier transform). These processes are all linear, so they can be interchanged with other linear operations. Since linear operations are interchangeable, the compressed signal is identical to an output signal when a pulse signal is supplied directly to the system. These processes are known as the signal compression method, originally proposed by Aoshima (Aoshima, 1984). For systems with a single input and a single output that include a nonlinear term, the signal compression method is known to identify the inertia moment or viscosity friction coefficient (Lee and Aoshima, 1989). When using the signal compression method, the response of linear and nonlinear elements can be divided so that the linear part can be extracted. Using the obtained impulse response, parameters of linear elements can be approximately acquired. That is, a comparison is made between the two Bode diagrams of the system transfer function and the impulse response of the linear element.

To determine the switching parameters, the values of inertia J and damping factor B of the whole system are obtained experimentally using the signal compression method (Table 3). Then the switching parameters are derived for the case of $c_1=4$ and $c_2=4$ to satisfy the existence condition of the sliding mode (Table 4).

A total of 4,000 sets of angle and velocity data were stored in the memory with a sampling period of 1 msec. The thresholds ε_1 and ε_2 were chosen as 0.5 for the quasi-sliding mode. The proportional gains $K_{p1}=K_{p2}=1$ were used to determine the control input before the sliding mode occurred. The values of the dead zones D_1 and D_2 were set equal to 0.5. Each value of M_{1i} in Table 4 was changed to M_{1di} within the dead zone. Figure 13 shows a step response under the sliding mode control with the preset dead zones in the error state space. The state trajectories were found faithfully follow to the switching line. This shows that the signal compression method is adequate for identifying parameters to obtain the switching input gains.

Figures 14 and 15 show the velocities of axis 1 under sliding mode control without and with the preset dead zone, respectively. The reduction of chattering around the steady state is obtained by

Table 3 Estimated parameters of control system.

	$J(kg \cdot m^2)$	$B(kg \cdot m^2/s)$
Axis 1	0.20438	1.2703
Axis 2	0.06162	0.7864

Table 4 Switching parameters of control system.

	α_i	M_{1i}	M_{2i}
Axis 1	0.5	0.0625 $s>0$ −0.1719 $s<0$	0.25
Axis 2	0.5	0.156 $s>0$ −0.0547 $s<0$	0.25

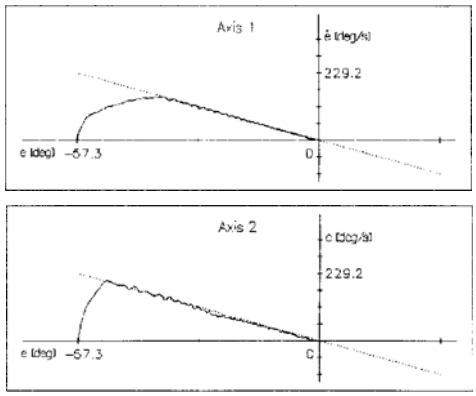

Fig. 13 State trajectory in error state space.

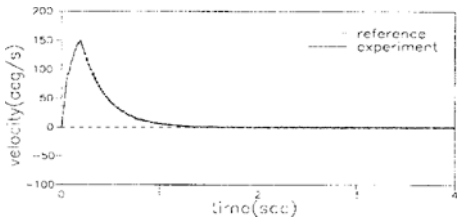

Fig. 14 Velocity of axis 1 without dead zone.

Table 5 Control gains for trajectory control.

	Axis 1		Axis 2	
α_i	−0.50	$s_1e_1>0$	−1.81	$s_2e_2>0$
	0.31	$s_1e_1<0$	0.50	$s_2e_2<0$
β_i	0.13	$s_1\dot{\theta}_{d1}>0$	0.19	$s_2\dot{\theta}_{d2}>0$
	−0.31	$s_1\dot{\theta}_{d1}<0$	−0.69	$s_2\dot{\theta}_{d2}<0$
M_{1i}	0.31	$s_1>0$	0.25	$s_2>0$
	−0.38	$s_1<0$	−0.31	$s_2<0$
M_{1di}	0.17	$s_1>0$	0.20	$s_2>0$
	−0.31	$s_1<0$	−0.20	$s_2<0$

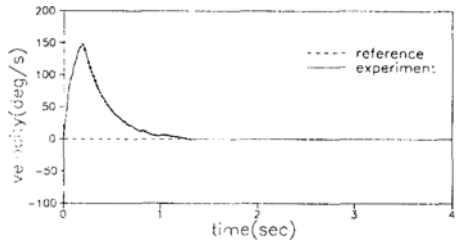

Fig. 15 Velocity of axis 1 with dead zone.

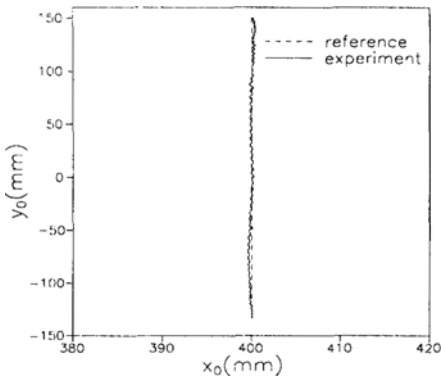

Fig. 16 Trajectory tracking by sliding mode control using larger M_{1di}.

the addition of the dead zone.

It was experimentally verified that the proposed algorithm, by decreasing the value of M_{1i} to that of M_{1di} within the preset dead zones, reduced chattering. To evaluate the effects of the control gain, the experiment was performed for the case of the larger values of M_{1di} as in Table 5. The experiment was done for a task where the end-effector moved in 1 Sec from the start point (400 mm, 150 mm) to the end point (400 mm, −130 mm) in the $x-y$ plane.

Table 6 Small gain for distrubance term.

	Axis 1		Axis 2	
M_{1i}	0.25	$s_1>0$	0.25	$s_2>0$
	−0.31	$s_1<0$	−0.25	$s_2<0$
M_{1di}	0.16	$s_1>0$	0.16	$s_2>0$
	−0.16	$s_1<0$	−0.16	$s_2<0$

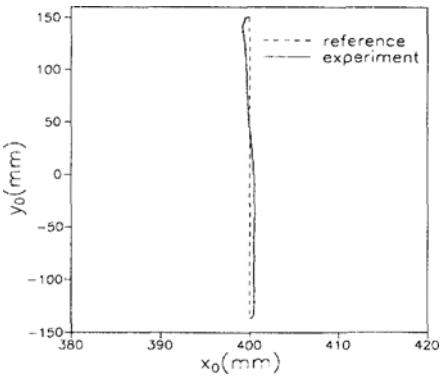

Fig. 17 Trajectory tracking by sliding mode control using small M_{1di}.

Figure 16 shows the tracking trajectory in the case of large M_{1di}. It was known that the end-effector follows the reference trajectory well, but the chattering becomes larger. To reduce the chattering, a smaller value M_{1di} was selected as in Table 6. Figure 17 shows the corresponding result: the tracking error becomes larger while the chattering becomes smaller. The larger tracking error is due to the fact that the smaller value M_{1di} does not sufficiently compensate for nonlinear terms such as friction force, backlash, etc. Therefore, the control gain M_{1di} within the preset dead zones should be selected by considering both the magnitude of chattering and allowable error.

A method to reduce both chattering and tracking error can be explained with Fig. 18. The control input gain M_{Li} is changed adaptively to between values of M_{Li} and M_{Hi} in the region of D_{Li} and D_{Hi}. Figure 19 shows the tracking trajectory for the values listed in Table 7. The maximum deviation from the desired trajectory is less than 0.8 mm in spite of neglecting all the nonlinear terms. Chattering and tracking error are smaller than those in Figs. 16 and 17. A comparison of trajectory tracking performance in Figs. 12

Table 7 Gains for continuous dead zone.

	Axis 1	Axis 2
M_{Hi}	0.4	0.4
M_{Li}	0.16	0.16
D_{Hi}	0.2	0.2
D_{Li}	0.075	0.075

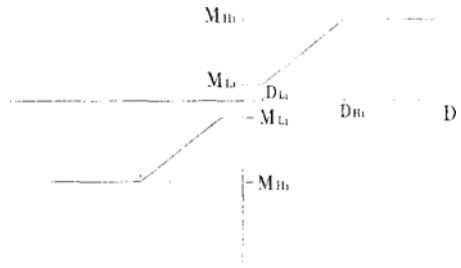

Fig. 18 Continuous control input within dead zone.

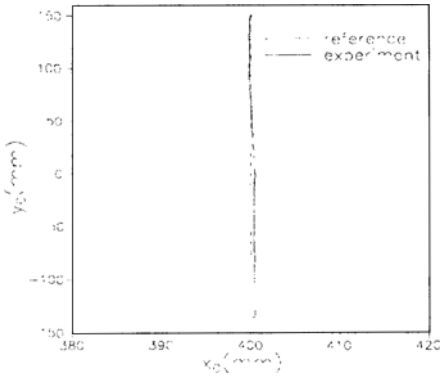

Fig. 19 Experimental results obtained by the proposed sliding mode control.

and 19 shows that the proposed sliding mode control is better than the PD control. Figures 20 and 21 show the tracking result of axes 1 and 2 in the joint coordinates. These results show that the proposed algorithm can provide reliable and robust tracking performance.

5. Conclusions

The trajectory tracking performance of a SCARA robot has been investigated using the proposed sliding mode control algorithm. It was shown, through simulations and experiments, that

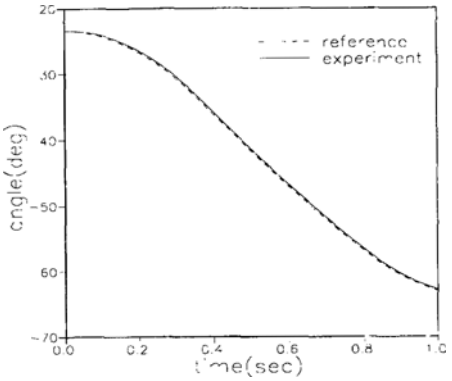

Fig. 20 Angle tracking of axis 1 by sliding mode control.

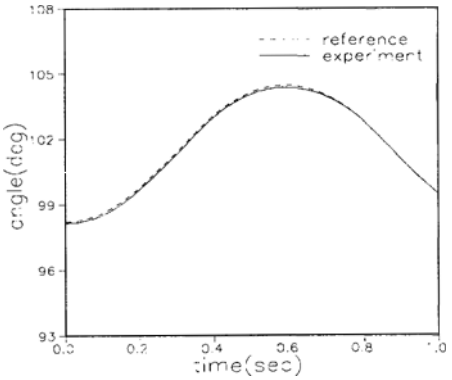

Fig. 21 Angle tracking of axis 2 by sliding mode control.

the proposed algorithm provides improved performance even though the unmodeled dynamics are considered as an external disturbance. The chattering related to the sliding mode control can be reduced to a negligible level by decreasing the switching parameter gains to smaller values when the state variables fall into a dead zone predetermined along the switching line. Prior to the implementation of the suggested algorithm, a dynamic simulator had been developed and was used for the determination of control gains and a dead zone. The dynamic simulator was also used in the comparison of the proposed algorithm and the computed torque method. The experimental results show that the proposed algorithm is superior to conventional ones and easily applicable to industrial robots.

Acknowledgment

This research was supported in part by the Korea Science and Engineering Foundation (KOSEF) through the Engineering Research Center for Net Shape and Die Manufacturing at Pusan National University and in part by the G7 project sponsored by the Ministry of Trade Industry and Energy (MOTIE).

References

Aoshima, N., 1984, "Measurement of Nonlinear Vibration by Signal Compression Method," *Journal of Acoustic Society Am.*, Vol. 76, No. 3, pp. 794~801.

Dong, Y. and Shifan, Xu, 1996, "Sliding Mode Control of Singular Perturbation Systems," *IEEE Int. Conference on System, Man and Cybernetics*, pp. 113~116.

Fu, K. S., Gonzalez, R. C., and Lee, C. S. G, 1987, *ROBOTICS: Control, Sensing, Vision and Intelligence*, McGraw-Hill.

Furuta, T. and Tomiyama, K., 1996, "Sliding Mode Controller with Time-Varying Hyperplane," *Proc. of the IEEE/RSJ Int. Conference on Intelligent Robots and Systems*, pp. 576~581.

Harashima, F., Hashimoto, H., and Maruyama, K., 1986, "Sliding Mode Control of Manipulator with Time-Varying Switching Surfaces," *Trans. of the Society of Instrument and Control Engineers*, Vol. 22, No. 3, pp. 335~342.

Hashimoto, H., Maruyama, K., and Harashima, F., 1987, "A Microprocessor-Based Robot Manipulator Control with Sliding Mode," *IEEE Trans. on Industrial Electronics*, Vol. 34, No. 1, pp. 11~18.

Lee, M. C. and Aoshima, N., 1989, "Identification and Its Evaluation of the System with a Nonlinear Element by Signal Compression Method," *Trans. of the Society of Instrument and Control Engineers*, Vol. 25, No. 7, pp. 729~736 (in Japanese).

Lee, M. C. and Aoshima, N., 1993, "Real Time Multi-Input Sliding Mode Control of a Robot Manipulator Based on DSP," *Proc. of the '93 Society of Instrument and Control Engineers*, pp. 1223~1228.

Lee, M. C., Son, K., Lee, J. M., Lee, M. H., Ahn, D. S., and Han, S. H, 1995, "Implementation of a New Sliding Mode Control for SCARA Robot," *Proc. of the '95 American Control Conference*, Vol. 2 of 6, pp. 1387~1391.

Nishimoto, K., 1985, "DSP and Its Application to Robot Control," *Journal of the Robotics Society of Japan*, Vol. 7 No. 3, 339~345.

Parra-Vega, V., Liu, Y., and Arimoto, S., 1994, "Variable Structure Robot Control Undergoing Chattering Attenuation: Adaptive and Nonadaptive Cases," *Proc. of the IEEE Int. Conference on Robotic and Automation*, pp. 1824~1829.

Slotine, J. J. E., 1985, "The Robust Control of Robot Manipulators," *Int. Journal of Robotics Research*, Vol. 4, No. 4, pp. 49~64.

Son, K., Jung, C. W., Lee, M. H., Lee, M. C., Lee, J. M., Ahn, D. S., and Han, S. H., 1994, "A Human-Robot Interface System Developed in PC's," *12th Journal of the Robotics Society of Japan Conference*, pp. 101~104.

Utkin, V. I., 1978, *Sliding Modes and Their Application in Variable Structure Systems*, Mir Publishers, Moscow.

Wang, J., Bailey, W. N., and Dodds, S. J., 1994, "A New Sliding Mode Approach to the Robust Control of Robotic Manipulators with Dynamic Uncertainties," *Proc. of the IEEE Int. Conference on Robotic and Automation*, pp. 2100~2105.

Young, K. D., 1978, "Controller Design for Manipulator Using Theory of Variable Structure Systems," *IEEE Trans. on System, Man and Cybernetics*, Vol. 8, No. 2, pp. 101~109.

Appendix

$$H_{11}=m_1 l_{c1}^2+I_1+m_2(l_1^2+l_{c2}^2+2l_1 l_{c2}\cos\theta_2)+I_2+(m_3+m_4)(l_1^2+l_2^2+2l_1 l_2\cos\theta_2)+I_4$$

$$H_{12}=H_{21}=m_2(l_{c2}^2+l_1 l_{c2}\cos\theta_2)+I_2+(m_3+m_4)(l_2^2+2l_1 l_2\cos\theta_2)+I_4$$

$$H_{22}=m_2 l_{c2}^2+I_2+m_3 l_2^2+m_4 l_2^2+I_4$$

$$H_{14}=H_{41}=H_{24}=H_{42}=-I_4$$

$$H_{33}=m_3+m_4$$

$H_{13}=H_{31}=H_{23}=H_{32}=H_{34}=H_{43}=0$

$h_{112}=-2m_2l_1l_{c2}\sin\theta_2-2(m_3+m_4)l_1l_2\sin\theta_2$

$h_{122}=-m_2l_1l_{c2}\sin\theta_2-(m_3+m_4)l_1l_2\sin\theta_2$

$h_{211}=m_2l_1l_{c2}\sin\theta_2+(m_3+m_4)l_1l_2\sin\theta$

$h_{212}=-h_{221}$

$=-0.5(m_2l_1l_{c2}\sin\theta_2+(m_3+m_4)l_1l_2\sin\theta_2)$

$G_1=G_2=G_4=0$

$G_3=-g(m_3+m_4)$, $g=9.8\text{m/sec}^2$

where,

ν_i : viscous friction coefficient of joint i

$ksgn(\dot{\theta}_i)$: Coulomb friction

θ_i : rotation angle at joint i

d_3 : translational displacement along axis 3

m_i : mass of link i

l_i : length of link i

l_{ci} : distance from base joint of link i to center of mass i

I_i : inertia of link i